Solution Structure of Mouse Cripto CFC Domain and Its Inactive Variant Trp107Ala†

Luisa Calvanese,‡,§ Angela Saporito,‡,|| Daniela Marasco,|| Gabriella D'Auria,§,|| Gabriella Minchiotti,⊥ Carlo Pedone,|| Livio Paolillo,§,|| Lucia Falcigno,*,§,|| and Menotti Ruvo*,||

Dipartimento di Chimica, Università Federico II, Complesso Universitario MSA, via Cintia 45, 80126 Napoli, Italy, Istituto di Biostrutture e Bioimmagini del CNR, via Mezzocannone, 16, 80134 Napoli, Italy, and Istituto di Genetica e Biofisica "Adriano B. Traverso" del CNR, via P. Castellino, 111, 80126 Napoli, Italy

Received June 29, 2006

We report here for the first time the solution structures at pH 3 and pH 6 of the synthetic CFC domain of mouse Cripto and of the point mutated variant W107A that is unable to bind to the Alk4 Cripto receptor. NMR data confirm that the CFC domain has a C1−C4, C2−C6, C3−C5 disulfide pattern and show that structures are rather flexible and globally extended, with three noncanonical antiparallel strands. His104 and Trp107 side chains protrude from a protein edge and are strongly exposed to solvent, supporting previous evidence of direct involvement in receptor binding. On the opposite molecule side, several nonpolar residues are gathered, forming a large hydrophobic patch that supposedly acts as interface with the cell membrane or the adjacent EGF-like domain. A second hydrophilic patch surrounding His104 and Trp107 is present only in the wild type variant, suggesting a possible involvement in modulating Alk4 recognition.

Introduction

Cripto is a membrane protein indicated as an important target of therapeutic intervention for the treatment of several widespread cancers, including breast, colon, and lung carcinomas.[1−4] The protein displays all the features of an oncogene,[3] being able to support survival, transformation, migration, and proliferation in a large variety of cell lines.[5,6] It is also highly overexpressed in many tumors, while it is poorly detectable in normal tissues.[7] Accordingly, induction of Cripto overexpression in transgenic mice causes hyperplasia and tumor formation in host tissues,[8,9] suggesting a direct molecular link with signaling pathways of uncontrolled cell growth. Cripto is expressed during pregnancy and lactation[10−12] and during early embryogenesis,[10] whereby it plays a crucial role in the specification of the anterior−posterior and left−right axis and in the formation of several organs.[13] In addition, it has also been described as a key regulator of stem cell fate[14−18] and as an important pro-angiogenic factor.[19] Two main signaling pathways have so far been identified for Cripto, both supporting cell survival. A first important pathway involves the activin receptor complex (comprising the Activin type II serine/threonine kinase receptor, ActRII, and the Activin type I serine/threonine kinase receptor, Alk4) and a number of proteins of the TGFβ family, including Nodal,[14,20−23] Vg1/Gdf1,[24] Gdf3,[25] Activin A,[26] Activin B,[1] and Lefty.[27] Current evidence indicates that Cripto performs an obligatory role as co-receptor for Nodal as well as for Gdf1 and Gdf3; indeed, binding of Nodal/Gdf1/Gdf3 to the activin receptor complex (Alk4/ActRIIB) occurs only in the presence of Cripto. Following receptor activation, Smad2 and Smad3 are phosphorilated and accumulate together with Smad4 in the nucleus to mediate transcriptional response. A second Nodal/Alk4-independent signaling pathway involves binding to Glypican-1 and the subsequent activation of phosphoinositol-3 kinase/Akt and the ras/mitogen-activated protein kinase intracellular cascade that, likewise, induces proliferation, migration, and growth.[28]

Structurally, Cripto is composed of two adjacent cysteine-rich motifs, the EGF-like and the CFC, of a N-terminal signal peptide and of a C-terminal hydrophobic region involved in the cell membrane attachment by a GPI anchor.[13] All these features identify a family of growth factors named EGF−CFC of which Cripto is the founding member.[13] The EGF-like and the CFC motifs are small domains of about 40 residues, each compacted by three internal disulfide bridges[29,30] that are deemed to fulfill distinct functional roles. Indeed, genetic experiments have demonstrated that the EGF-like domain binds to Nodal, while the CFC binds to the Alk4 receptor.[1,31] Consistently, mutations in the EGF-like motif, which prevent Nodal binding, or mutations in the CFC motif that affect Alk4 recognition,[22] both block the receptor activation and lead to cell growth inhibition. A further mechanism by which Cripto can induce carcinogenesis involves direct binding to Activins, soluble ligands that normally bind to the Alk4/ActRIIB receptor complex in a Cripto-independent fashion and promote tumor-suppressive signals in normal tissues.[32] Cripto reportedly interacts with Activins,[1,26] and it has been postulated that this interaction could impair the Activin growth suppressive activity by competition with Alk4[1] or Nodal,[26] therefore, inducing cell survival. Whether Cripto binds to Activin A or B is still a matter of debate; however, it has been shown that monoclonal antibodies (MAbs) raised against the CFC domain[1] are able to prevent or reduce tumor formation in xenograft models and are promising drug candidates for further clinical development as effective tumor-suppressive therapeutics.[1,33,34] Anti-EGF-like MAbs have also been successfully utilized to prevent tumor development in vivo and to inhibit the growth of established tumors of colon xenografts in mice, though their use seems to be more effective in combination with cytotoxic drugs.[2,35] Remarkably, these observations suggest that, although intricate multiprotein complexes are formed and complicated interplays between several interacting partners are activated during all phases of carcino-

* To whom correspondence should be addressed. Tel.: +39-081-2536644 (M.R.); +39-081-674295 (L.F.). Fax: +39-081-2534574 (M.R.); +39-081-674090 (L.F.). E-mail: menotti.ruvo@unina.it (M.R.); lucia.falcigno@unina.it (L.F.).

† Coordinates have been deposited in the PDB with accession number 2j5h. NMR data for CFC at pH 6 are deposited at BMRB with accession number 7299.

‡ These authors contributed equally to this work.

§ Università Federico II.

|| Istituto di Biostrutture e Bioimmagini del CNR.

⊥ Istituto di Genetica e Biofisica "Adriano B. Traverso" del CNR.

10.1021/jm060772r CCC: $33.50
Published on Web 11/01/2006

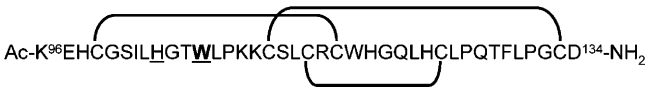

Figure 1. Amino acid sequence of mouse Cripto 96−134 CFC domain. Trp107 and His104 residues involved in Alk4 binding are underlined. Trp107 mutated to alanine in CFC-Mut is also shown in bold.

genesis, Cripto domains, and particularly CFC, have a decisive role and represent unique targets to fight severe and very aggressive tumor diseases.[1]

Recently, the disulfide bridge structure of human CFC has been experimentally determined to be a C1−C4, C2−C6, C3−C5 pattern.[30] In the same report, a 3D structure for CFC has been predicted, implying that small serine protease inhibitors, known as PMP-C, having the same pattern of disulfide connections, are remote homologues of CFC. In such a model, the largest loop connecting Cys115 and Cys128 (human numbering), contains several residues responsible of Alk4 interaction, notably His120, Trp123, and Pro125.[1,22,36,37] ELISA assays carried out with synthetic domains have shown that substitution of Trp107 with alanine in mouse CFC (corresponding to Trp123 in the human sequence) totally abolishes binding to Alk4, while the change of His104 (His120 in the human variant) only partially suppresses receptor recognition.[31] A comparative CD analysis has also shown that both mutants adopt slightly distorted secondary structure, suggesting that not only side-chain contacts, but also appropriate conformations contribute to receptor recognition and binding.[31] Therefore, the knowledge of the CFC structure and of the structural determinants for Alk4 and Activin recognition is of primary importance for the development of new tumor suppressive agents and for further elucidation of the molecular mechanisms underlying the Cripto-dependent tumor formation and progression. To this aim, we have undertaken an extensive conformational study by NMR of the chemically synthesized CFC domain of mouse Cripto,[31] spanning residues 96−134 (Figure 1), and of the inactive variant Trp107Ala, here named CFC-Mut. The study has been performed in water at both acidic pH, to facilitate the NMR assignment, and at pH 6 to approach the physiological environment. Our NMR studies are the first to be reported on this family of proteins and can provide the molecular basis for a better comprehension of the receptor recognition properties.

Results and Discussion

The NMR analysis of Cripto CFC domains has been carried out on the synthetic polypeptides prepared and refolded as described in Marasco et al.[31] In the same report, the CD analysis of CFC and CFC-Mut, performed under different pH conditions, has shown that the molecules do not assume canonical conformations, although the curves are indicative of organized structures with mixed alpha and beta structure contributions.[31]

NMR Analysis and Molecular Modeling of CFC and CFC-Mut in H_2O/D_2O 90/10 (v/v) at pH 3. Proton chemical shifts of CFC and CFC-Mut in H_2O/D_2O 90/10 (v/v) at pH 3 are reported in Table S1 and Table S2 of the Supporting Information.

A preliminary structural diagnosis was obtained by comparing the CFC and CFC-Mut αCH proton chemical shifts to random coil values[38] for each residue. As shown in Figure 2, most residues show positive deviations from random coil values, more marked in the central part of the molecule, suggesting the presence of *β*-sheet structures. This structural diagnosis is consistent with the NOE pattern. NOE effects such as α_i-NH_{i+1} appear stronger than the corresponding NH_i-NH_{i+1}, nicely confirming the occurrence of extended conformations. Some unambiguous interstrand NOE contacts were also observed: αCH Cys115−αCH Cys124 and αCH Cys99−αCH Cys117, for both analogues. These contacts confirm that the disulfide bridge disposition is consistent with that reported in previous investigations.

A set of 241 experimental NOE constraints for CFC (136 intraresidual, 87 sequential, and 18 long-range) and 242 for CFC-Mut (125 intra-residual, 80 sequential, and 37 long-range) were used for structure calculations by DYANA/Amber programs (Tables 1 and 2).[39] Additional constraints were inserted for Φ dihedral angles of those residues showing large $^3J_{NH-\alpha CH}$ coupling constants, measured by DQFCOSY spectra. In particular, nine and seven torsion angle restraints were used for CFC and CFC-Mut, respectively. The best 10 structures (see Experimental Section for details), with a residual restraint energy lower than −196 kcal/mol for CFC and −81.0 kcal/mol for CFC-Mut, were selected to represent the polypeptide solution structures. The peptide adopts a flexible structure with a backbone mean global root-mean-square deviation (rmsd) of 6.25 ± 1.56 Å for CFC and 4.46 ± 1.17 Å for CFC-Mut. The most ordered peptide regions correspond to the segment C99−C115, C115−C124, and C124−C133. Backbone mean global rmsd for the superposition of the final ten structures are reported in Table 2.

The molecular model of CFC shows an ellipsoidal compact shape with approximate dimensions of 24 Å × 20 Å × 18 Å (Figure 3a). The molecular model of CFC-Mut also shows an ellipsoidal prolate shape but with approximate dimensions of 30 Å × 14 Å × 16 Å (Figure 3b). The molecules are globally extended with three antiparallel strands connected by disulfide bridges. Pro109 and Pro131 residues are located at corners. The first two strands are more extended than the third one, which is bent in the segment 118−126, mainly constituted by hydrophobic residues. A difference observed between CFC and CFC-Mut molecular models regards the orientation of the C-terminal tail that points to the first strand in the case of CFC-Mut.

The disulfide bridges show multiple conformations[40] in all final structures, but this does not substantially change the structure of the backbone. The first disulfide bridge in the sequence is established between Cys99−Cys117 and links the N-terminal segment to the central strand of the model. This bridge has alternative conformations according to the χ_3 angle value: "left-handed" (6 structures out of 10) and "right-handed" (4 structures out of 10) that correspond to mean values of the angle χ_3 of −82° and of +82°, respectively. The same bridge for CFC-Mut shows multiple conformations with five "left-handed" structures ($\chi_3 = -68°$) and five "right-handed" structures ($\chi_3 = +68°$). The mean distance αCH Cys99−αCH Cys117 is equal to 3.2 Å and to 3.9 Å, for CFC and CFC-Mut, respectively. The disulfide bridge Cys115−Cys124 links the second and the third strand and is arranged orthogonally to the near bridge S−S Cys99−Cys117. This bridge also shows multiple conformations with five "left-handed" structures ($\chi_3 = -80°$) and five "right-handed" structures ($\chi_3 = +82°$) for CFC and with four "left-handed" structures ($\chi_3 = -83°$) and six "right-handed" structures ($\chi_3 = +93°$) for CFC-Mut. The disulfide bridge is characterized by a short mean distance αCH Cys115−αCH Cys124 equal to 2.8 Å for both polypeptides. The third bridge, Cys112−Cys133, links the C-terminal residues to the loop between the first two strands. It is arranged parallel to the second bridge in the molecular model for CFC and orthogonally to the bridge S−S Cys115−Cys124 for CFC-Mut. The χ_3 angle values are −106° and −74° for five structures and +78° and +90° for the other five structures for CFC and

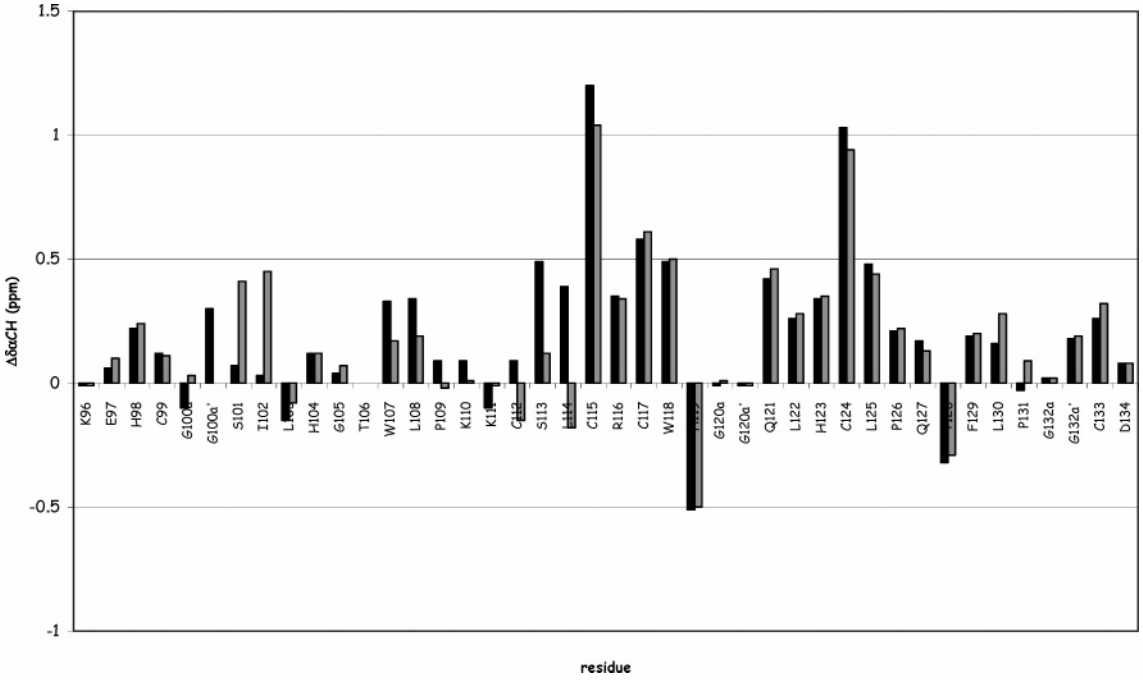

Figure 2. Chemical shift deviations from the random-coil values for αCH protons[38] at pH 3 of CFC (black bars) and CFC-Mut (gray bars).

Table 1. NMR Structure Determination Statistics

	CFC pH 3	CFC-Mut pH 3	CFC pH 6	CFC-Mut pH 6
		NMR Restraints		
distance restraints	241	242	179	167
intraresidue	136	125	76	96
sequential ($\|i-j\|=1$)	87	80	55	44
medium-range ($1<\|i-j\|\leq 4$)	18	37	48	27
torsion angle restraints	9	7	0	13
mean global backbone rmsd (96−134)	6.14 ± 1.22 Å	5.41 ± 1.19 Å	5.22 ± 0.90 Å	5.25 ± 1.19 Å
mean global heavy rmsd (96−134)	7.78 ± 1.19 Å	6.79 ± 1.18 Å	6.88 ± 0.96 Å	6.38 ± 1.18 Å
		Violation Statistics[a] (40 Structures)		
DYANA TF (Å^2)	0.56 ± 0.17	1.58 ± 0.37	3.13 ± 1.16	0.94 ± 0.21
		Residual Distance Constraint Violations (Å)		
number > 0.2 Å	1	4	6	4
sum	0.09	0.17 ± 0.04	0.18 ± 0.12	0.24 ± 0.02
maximum	0.25	0.47 ± 0.09	0.71 ± 0.19	0.30 ± 0.05

[a] Values are the average ± standard deviation for the ensemble of the best 40 structures obtained by REDAC strategy.

CFC-Mut, respectively. The average distance αCH Cys112−αCH Cys133 is equal to 6.0 Å for CFC and to 5.8 Å for CFC-Mut.

It is worth noticing that, in the CFC molecular model, the side chains of His104 and Trp107 residues, involved in the binding with the receptor,[22,30,31,41] are exposed to the solvent and surrounded by positively charged residues both above (Lys96, His98, His119) and below (Lys110, Lys111). In addition, a large hydrophobic patch spanning residues 122−130, which is believed to be responsible for the interaction of Cripto with the cellular membrane or is part of the interface with the adjacent EGF-like domain,[30] is found opposite to the binding site.

NMR Analysis and a Molecular Modeling in H_2O/D_2O 90/10 (v/v) at pH 6. The conformational analysis via NMR of both peptides was performed at pH 6 to approach physiological conditions and, thus, to monitor possible structural changes with respect to acid pH values. Proton chemical shifts of CFC and CFC-Mut in H_2O/D_2O 90/10 (v/v) at pH 6 are reported in Tables S3 and S4 of the Supporting Information. As a result of the fast exchange phenomena with water, some NH resonances were missing. In these cases, the amino acid spin systems were assigned by inspection of the high field correlation regions in the 2D maps (Figure 4). The αCH chemical shift deviations from random coil values[38] versus residue number (Figure 5) show a trend similar to that observed for both peptides at pH 3. However, the deviations at pH 6 are very large, indicating a higher percentage of ordered conformers at pH 6 than at pH 3. A set of 179 experimental constraints from NOE data for CFC (76 intra-residual, 55 sequential, and 48 long-range) and 167 for CFC-Mut (96 intra-residual, 44 sequential, and 27 long-range) were used for molecular model calculations by the DYANA/Amber (Tables 1 and 2).[39] Additional 13 torsion angle constraints were inserted for CFC-Mut. The best 10 structures (see Experimental Section for details), with a residual restraint energy lower than −67.5 kcal/mol for CFC and −90.3 kcal/mol for CFC-Mut, were selected to represent the peptide solution structures (Figures 3c and 3d). The peptide adopts a flexible structure with a backbone mean global root-mean-square deviation (rmsd) of 4.75 ± 1.07 Å for CFC and 5.00 ± 1.15 Å

Table 2. AMBER Structural Statistics

	CFC pH 3[a]	CFC-Mut pH 3[a]	CFC pH 6[a]	CFC-Mut pH 6[a]
	Residual Distance Constraint Violations (Å)			
$0.2 < d \leq 0.3$	5.9 ± 2.3	5.8 ± 2.9	6.1 ± 1.9	6.0 ± 1.7
$0.3 < d \leq 0.4$	1.4 ± 1.1	2.2 ± 1.5	2.6 ± 1.8	2.3 ± 1.2
$0.4 < d \leq 0.5$	0.7 ± 0.8	2.0 ± 1.1	2.1 ± 1.4	0.7 ± 0.8
maximum violation	0.40 ± 0.07	0.58 ± 0.14	0.56 ± 0.16	0.42 ± 0.09
	AMBER Energies (kcal mol^{-1})			
distance constraint	14.5 ± 2.42	24.8 ± 5.45	24.3 ± 6.55	18.8 ± 3.16
van der Waals	-181.4 ± 41.4	-185.9 ± 7.88	-195.0 ± 9.58	-183.8 ± 10.4
total	-216.5 ± 16.3	-95.31 ± 14.2	-130.6 ± 33.9	-115.2 ± 24.0
	RMSD to the Averaged Coordinates[b] (Å)			
backbone (96−134)	6.25 ± 1.56	4.46 ± 1.17	4.75 ± 1.07	5.00 ± 1.15
all heavy (96−134)	7.60 ± 1.58	5.75 ± 1.38	6.05 ± 1.21	5.99 ± 1.27
backbone (99−107)	2.45 ± 0.61	2.24 ± 0.56	1.99 ± 0.51	2.35 ± 0.59
all heavy (99−107)	4.22 ± 0.90	3.45 ± 0.85	3.30 ± 0.78	3.31 ± 0.91
backbone (110−115)	1.63 ± 0.39	1.56 ± 0.45	1.64 ± 0.40	1.53 ± 0.56
all heavy (110−115)	3.19 ± 0.58	3.21 ± 0.82	3.26 ± 0.71	2.75 ± 0.87
backbone (99−115)	3.73 ± 0.84	2.91 ± 0.76	2.79 ± 0.77	3.03 ± 0.81
all heavy (99−115)	5.01 ± 1.00	4.24 ± 0.99	4.15 ± 0.90	3.95 ± 0.99
backbone (115−124)	3.99 ± 1.08	1.82 ± 1.09	3.35 ± 0.76	1.93 ± 0.82
all heavy (115−124)	2.47 ± 1.10	3.35 ± 1.08	1.89 ± 0.63	3.29 ± 0.78
backbone (124−133)	4.39 ± 1.20	2.11 ± 0.72	3.62 ± 0.77	2.33 ± 0.52
all heavy (124−133)	4.35 ± 0.88	3.20 ± 1.10	4.12 ± 1.03	3.49 ± 0.79

[a] Average value for the ten selected energy minimized conformers. [b] Average coordinates of the selected energy minimized conformers after superposition for the best fit of the atoms of residues indicated in parentheses.

for CFC-Mut. Despite the conformational flexibility, indicated by the high rmsd, some structural features systematically occur in short peptide regions, determined by locally reduced conformational dispersion. As observed at pH 3, the most ordered regions of the peptides correspond to the segment C99−C115, C115−C124, and C124−C133. Backbone mean global rmsd for the superposition of the final 10 structures are reported in Table 2.

Molecular models show an ellipsoidal prolate shape with approximate dimensions of 32 Å × 12 Å × 17 Å and 30 Å × 14 Å × 10 Å, for CFC and CFC-Mut, respectively. The folding of both molecules is globally extended with the presence of three antiparallel strands linked by the disulfide bridges and connected through loops larger than those observed at acid pH. The first and the central strands are more regular than the third one. With regard to CFC-Mut, two structures out of 10 show short regular strands of antiparallel β-sheet in the 114−115/124−125 and 115−117/122−124 segments. Both molecules show the loop 107−112 centered on a proline (Pro109) larger in CFC-Mut than in CFC molecular model. Differently from CFC, the C-terminal tail points to the first strand in the case of CFC-Mut. It is worth noticing that two NOE contacts, 4.35−4.57 ppm and 4.35−2.74 ppm, were not inserted in structure calculations due to an ambiguity of assignment. In fact, both the αCH proton resonances of P109 and P131 are found at 4.35 ppm, while αCH and βCH_2 of D134 resonate at 4.57 and 2.74 ppm, respectively. On the basis of the CFC-Mut molecular model, these NOEs can be assigned, a posteriori, to P109/D134 contacts.

As observed at pH 3, the disulfide bridges show multiple conformations[40] in the 10 final structures, but this does not considerably affect the backbone structure. For CFC, the first Cys99−Cys117 disulfide bridge has alternative conformations according to χ_3 angle value: "left-handed" (6 structures out of 10) and "right-handed" (4 structures out of 10) that correspond to mean values of the χ_3 angle of −78° and +89°, respectively. The same bridge for CFC-Mut shows multiple conformations with four "left-handed" structures ($\chi_3 = -57°$) and six "right-handed" structures ($\chi_3 = +77°$). The mean distance αCH Cys99−αCH Cys117 is equal to 4.7 Å and to 3.1 Å for CFC and CFC-Mut, respectively. The second disulfide bridge, Cys115−Cys124, is arranged orthogonally to the near S−S Cys99−Cys117 bridge. The χ_3 angle values are −71° and −85° for five structures and +72° and +87° for the remaining five structures for CFC and CFC-Mut, respectively. It is characterized by a short αCH Cys115−αCH Cys124 mean distance equal to 4.0 Å for CFC and to 2.2 Å for CFC-Mut. The third disulfide bridge, Cys112−Cys133, is arranged parallel to the second bridge in the molecular model for CFC and orthogonally to the S−S Cys115−Cys124 bridge for CFC-Mut. This bridge also shows multiple conformations with two "left-handed" structures ($\chi_3 = -102°$) and eight "right-handed" ($\chi_3 = +87°$) structures for CFC and with six structures "left-handed" ($\chi_3 = -103°$) and four "right-handed" ($\chi_3 = +95°$) structures for CFC-Mut. The average distance αCH Cys112−αCH Cys133 is equal to 5.4 Å for CFC and to 5.7 Å for CFC-Mut. As already observed for CFC molecular model at pH 3, also at pH 6, the side chains of His104 and Trp107 residues, involved in the binding with the receptor,[22,30,31] are strongly water exposed. NMR data, αCH proton chemical shift deviations, from random coil values and NOE effects indicate a higher percentage of ordered conformations at pH 6 than at pH 3, as expected. In particular, although the total NOE number is higher at pH 3 than at pH 6, the percentage of long-range NOEs increases at physiological conditions for both sequences (27% vs 7% for CFC and 16% vs 15% for CFC-Mut). Moreover, the decrease of the total NOE number at pH 6 is mainly due to the lack of several NH resonances and to the related backbone NOE effects.

In Figure 6, Connolly surfaces, computed for the average structures of CFC and CFC-Mut at both pH 3 and pH 6, are reported. In these representations, a hydrophobic patch located at a region opposing the binding site is clearly visible. This patch is consistently wide in more than 60% of the final selected structures, suggesting that it can really have a role in the recognition of other hydrophobic surfaces derived by the adjacent EGF-like, by cell membrane,[30] or by other soluble protein partners like Activins. Our data, for wild type CFC, are indicative of the occurrence of discrete hydrophilic patches above (Lys96, His98, His119) and below (Lys110, Lys111) the binding site. Surprisingly, a similar assembling of hydrophilic/hydrophobic residues is not observed in the CFC-Mut Connolly surfaces (at both pH 3 and pH 6), suggesting a possible

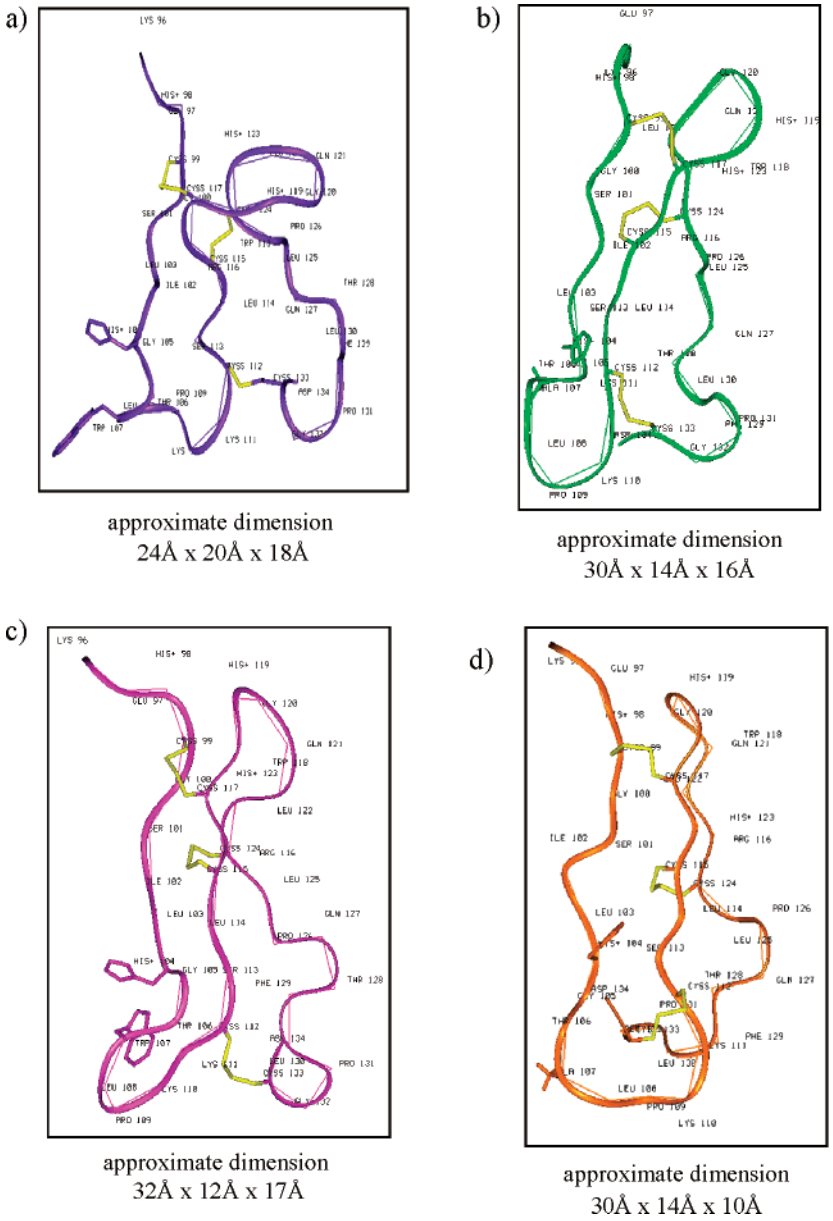

Figure 3. Ribbon representation of DYANA/AMBER average molecular models: (a) CFC pH 3 in violet; (b) CFC-Mut pH 3 in green; (c) CFC pH 6 in fuchsia; and (d) CFC-Mut pH 6 in orange. The side chains of Trp107 and of His104 are shown.

involvement of these residues in modulating the binding to Alk4. Moreover, as a consequence of the C-terminal tail found closer to the first strand in CFC-Mut molecular models, a short-range interaction between His104 and Asp134 appears in more than 50% of the final selected structures. This subtle structural difference, along with the hydrophilic region surrounding the Alk4 binding site in the wild type variant, could significantly contribute to the striking differences in Alk4 binding capacities exhibited by the two domains.

Conclusion

We report for the first time the solution structural characterization of isolated mouse Cripto CFC domains at pH 3 and pH 6. Cripto, as other members of the EGF−CFC proteins, contains two small adjacent motifs that are believed to fulfill distinct functions. The EGF-like domain, also found in other functionally unrelated proteins,[42] binds to soluble co-ligands through very few residues (Gly71 and Phe78, mouse numbering) and an unique fucose modification on Thr82.[43] Similarly, the CFC seems to bind Alk4 essentially via the side chains of His104 and Trp107.[22,30,31] Both interactions have been demonstrated to be mutually independent and self-sufficient, clearly indicating that isolated domains actually are functionally distinct. Remarkably, both domains are able to spontaneously refold to form the correct disulfide structure,[29,31] suggesting also a prominent structural independence. On these grounds, the characterization of the 3D-structure of EGF-like and CFC as isolated domains can be carried out, yet keeping in mind that quaternary interdomain interactions can occur in vivo to modulate more complex protein activities.

The molecular models of wild type mouse CFC and of the inactive variant bearing a single amino acid substitution on Trp107 as determined in solution by NMR at nearly neutral pH, do not show canonical structures, as previously evidenced by CD analysis.[32] All the determined structures show a globally extended folding and, as expected, they appear generally more structured at physiological pH values than under acidic conditions. The overall topology is determined by the presence of the three bridges, Cys99−Cys117, Cys115−Cys124, and Cys112−Cys133 that, in all the cases, show an equal distribution

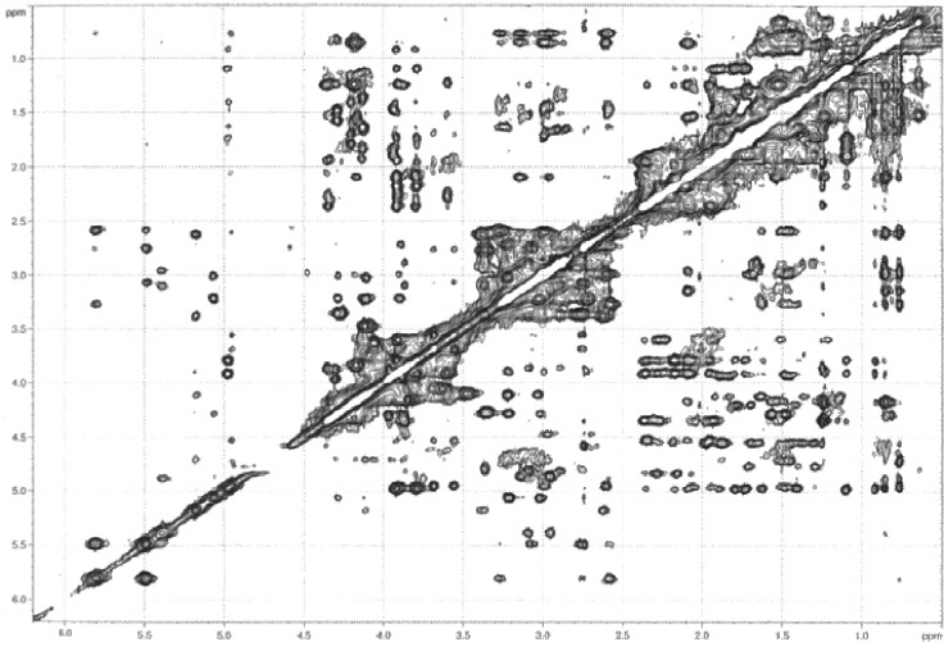

Figure 4. High-field correlation region of 200 ms NOESY spectra of CFC acquired in H_2O/D_2O 90/10 (v/v), at 700 MHz, 298 K at pH 3.

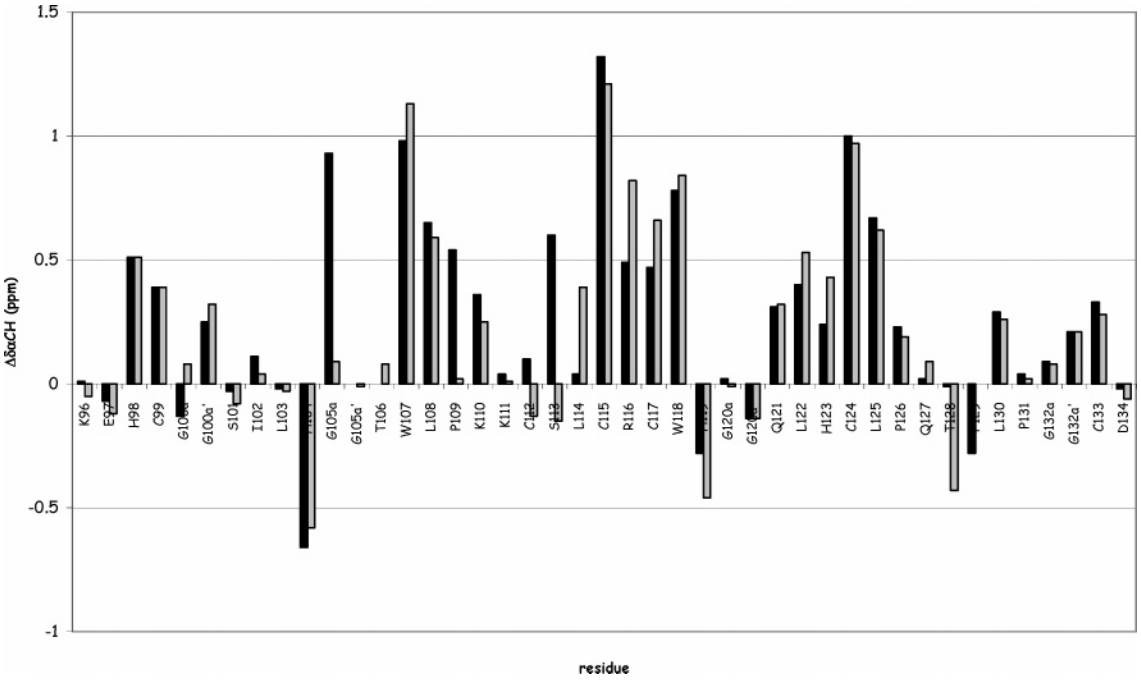

Figure 5. Chemical shift deviations from the random-coil values for αCH protons[38] at pH 6 of CFC (black bars) and CFC-Mut (gray bars).

among "left-handed" ($\chi_3 = -90° \pm 30°$) and "right-handed" ($\chi_3 = +90° \pm 30°$) conformations.[40] Interestingly, the presence of these multiple conformations around the S−S bonds does not substantially affect the structure of the backbone and, consequently, of the overall structures.

The calculated structures are not as compact as proteolysis experiments and the presence of the disulfide bridges would suggest, nor at pH 3 or at pH 6. Indeed, both the wild type and the Trp107Ala mutant display quite dynamic structures characterized, on the edges, by large flexible loops restrained by the disulfide bridges and, in the central core, by mostly noncanonical strands. This outcome is not really surprising, considering that small disulphide-rich proteins tend often to assume less regular secondary structures as compared to larger, more organized proteins.[40]

Significantly, the calculated structures of CFC, even at acidic pH, show that His104 and Trp107 are solvent exposed and in the main are iso-oriented, thus prone to binding with external partners, such as the Alk4. On the contrary, in the CFC-Mut calculated structures, the His104 and Ala107 side-chains, although solvent-exposed, are in general not well iso-oriented, with His104 pointing toward the C-terminal tail.

In the region near to the binding site in the CFC structures, several positively charged residues are also gathered that could thereby contribute to protein−protein interactions. Structural data also confirm the presence of a previously predicted[30] hydrophobic patch on the molecule side opposite to the Alk4 binding site. Indeed, Foley et al. suggested functional and sequence similarities of Cripto with the Von Willebrand Factor C-like domain of Jagged 2 for which no structural data are

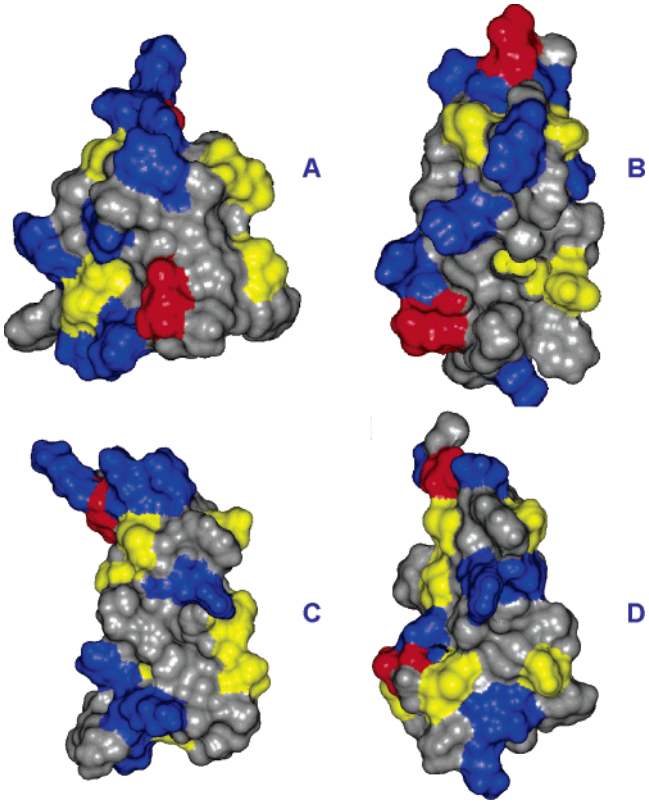

Figure 6. Connolly surfaces comparison of CFC and CFC-Mut molecular models. (A) CFC at pH 3; (B) CFC-Mut at pH 3; (C) CFC at pH 6; and (D) CFC-Mut at pH 6. Residues are colored as follows: acid (red), basic (blue), polar (yellow), and hydrophobic (gray). The hydrophilic patch around Trp107 and His104 is visible in the structure of CFC at pH 6 (C).

available.[30] In the same study, structural analogies of the CFC with PMP-C, a small serine protease inhibitor having the same disulfide connectivity, were also unveiled and used to build a model of the 3D structure of human CFC. While this theoretical model gives an account of the general domain folding and also predicts the hydrophobic patch, in light of our experimental data, it does not seem to properly depict all the domain conformational features.

The reason why these protein regions display such a broad conformational freedom is at present still unknown, and the available data do not support any convincing hypothesis. We can thereby not exclude a role of the adjacent EGF-like domain or of cellular environments in a structure stabilization, nor, by converse, an intrinsic structural flexibility that could explain the capacity to establish such a vast network of interactions, many of which have yet to be uncovered.

Experimental Section

NMR Analysis: NMR characterization was performed H_2O/D_2O 90:10 (v/v) at 298 K and/or 308 K for both the peptides CFC and CFC-Mut. Samples were prepared by dissolving about 4 mg of each peptide in 600 μL of H_2O/D_2O (90/10 v/v). D_2O was purchased by Sigma Aldrich (99.96% D). Final concentrations were 1.5 mM for each sample. The pH values, measured in pure water solutions, were 3. To this value of pH, a first series of NMR spectra was recorded, for both peptides, to obtain structural information in favorable conditions for NMR analysis. Subsequently, by means of proper additions of 0.12 M NaOH, the pH of both solutions was increased. In particular, the pH of both solutions turned out to be equal to 6. Therefore, a further series of NMR experiments were carried out on these samples to obtain structural information in conditions close to the physiological ones.

One- and two-dimensional (2D) NMR spectra were acquired on a DRX Bruker spectrometer, operating at a proton frequency of 700 MHz and located at Magnetic Resonance Center (CERM), University of Florence, Sesto Fiorentino, Italy. 2D experiments, such as total correlation spectroscopy (TOCSY),[44] nuclear Overhauser effect spectroscopy (NOESY),[45] and double quantum-filtered correlated spectroscopy (DQFCOSY)[46] were recorded by the phase-sensitive States−Haberkorn method.[47] The data file generally consisted of 512 and 2048 (4096 for DQFCOSY) data points in the $\omega 1$ and $\omega 2$ dimensions, respectively. TOCSY experiments were acquired with a 70 ms mixing time, while NOESY experiments were acquired with 100 and 200 ms mixing times. The water resonance was suppressed by the use of gradients.[48]

Chemical shifts were referred to internal sodium 3-(trimethylsilyl) propionate 2,2,3,3-d4 (TSP). Free induction decays (FIDs) were multiplied, in both dimensions, with shifted sine-bell or Gaussian weighting functions and data points were zero filled to 1K in $\omega 1$ prior to Fourier transformation. Spectra were analyzed by using NMRPipe/NMRView programs.[49,50] According to Wüthrich,[51] identification of amino acid spin systems was performed by comparison of TOCSY and DQFCOSY, while sequential assignment was obtained by the analysis of NOESY spectra. NOE intensities were evaluated by integration of cross-peaks in the 200 ms NOESY spectra, processed by NMRPipe, using the NMRView software.[50] They were then converted into interproton distances by the use of the CALIBA program,[52] based on the $1/r^6$ relationship for rigid molecules. P126 geminal δ,δ' protons and G132 geminal $\alpha-\alpha'$ protons for CFC at pH 3 and at pH 6, respectively, and C115 geminal $\beta-\beta'$ protons and G105 geminal $\alpha-\alpha'$ protons for CFC-Mut at pH 3 and at pH 6, respectively, were chosen as reference with a distance of 2.2 Å in each case.

Computational Methods: Torsion angle dynamics calculations were carried out by the DYANA program.[39] The library program was modified for the N- and C-terminal residues. Three-dimensional structures of both peptides were obtained using interproton distances evaluated from NOEs as upper limits, without use of stereospecific assignments. Additional constraints were used for Φ dihedral angles of those residues showing large values of $^3J_{NH-\alpha CH}$ ($\geq$9 Hz).[53] In those cases, Φ angles were set to $-120°$ with a tolerance of $\pm 10°$. Forty conformers were calculated with the standard parameters of the DYANA program. All of these conformers showed a sufficient agreement with experimental constraints (lowest target function (TF) value is 6.88 ± 5.21 Å^2 and 22.96 ± 15.45 for CFC at pH 3 and at pH 6, respectively; 14.59 ± 12.13 Å^2 and 7.66 ± 4.28 for CFC-Mut at pH 3 and at pH 6, respectively; the mean global backbone rmsd is 6.92 ± 1.27 Å for CFC at pH 3, 6.05 ± 1.06 Å for CFC at pH 6, 6.30 ± 0.96 Å for CFC-Mut at pH 3, and 6.38 ± 1.03 Å for CFC-Mut at pH 6. To improve convergence, the redundant dihedral angle constraints (REDAC)[54] strategy was also employed, and 100 more structures were calculated by carrying out five REDAC cycles for the analogues. Dihedral angle constraints were created with an ang-cut for the TF equal to 0.8 Å^2 in the first step, 0.6 Å^2 in the second, and 0.4 Å^2 in the third. In the fourth step, the structures were calculated with the constraints previously established. In the final step, no other dihedral angle constraints were created, and the structures were minimized at the highest level by use of all the experimental restraints.

The REDAC structures are indeed more compatible with the experimentally obtained data. Each structure shows few violations greater than 0.2 Å from the experimentally derived restraints: 1 versus 241 and 6 versus 179 for CFC at pH 3 and at pH 6, respectively, and 4 versus 242 and 4 versus 167 for CFC-Mut at pH 3 and at pH 6, respectively. For all the peptides, the 40 DYANA structures with the lowest values of TF (average value $= 0.56 \pm 0.17$ Å^2 for CFC at pH 3, 3.13 ± 1.16 Å^2 for CFC at pH 6, 1.58 ± 0.37 Å^2 for CFC-Mut at pH 3, 0.94 ± 0.21 Å^2 for CFC-Mut at pH 6; mean global backbone rmsd $= 6.14 \pm 1.22$ Å for CFC at pH 3, 5.22 ± 0.90 Å for CFC at pH 6, 5.41 ± 1.19 Å for CFC-Mut at pH 3, 5.25 ± 1.19 Å for CFC-Mut at pH 6) were subjected to restrained energy minimization by use of the SANDER module of the AMBER 6.0 package.[55,56] The 1991 version of the force field

was used,[57] with a distance-dependent dielectric constant $\epsilon(r)$. A distance cutoff of 12 Å was used in the evaluation of nonbonded interactions. Distance restraints were applied as a flat well with parabolic penalty within 0.5 Å outside the upper bound; a linear function beyond 0.5 Å with a force constant of 16 kcal mol^{-1} $Å^{-2}$ was used. The restrained energy minimization was carried out with a total of 2000 steps of conjugated gradient minimization, after 200 of steepest descent, for each analogue. The best structures in terms of the fitting with experimentally derived restraints were selected from those with a residual restraint energy lower than −196 kcal mol^{-1} and −67.5 kcal mol^{-1} for CFC at pH 3 and at pH 6, respectively, and −81.0 kcal mol^{-1} and −90.3 kcal mol^{-1} for CFC-Mut at pH 3 and at pH 6, respectively, to represent the peptides' solution structures. The molecular graphics program MOLMOL[58] was employed to perform the structural statistics analysis.

Acknowledgment. The Consorzio Interuniversitario Risonanze Magnetiche di Metallo Proteine Paramagnetiche (CIRMMP) for providing access to the high field instrumentation available at CERM, Firenze, the Associazione Italiana Ricerca sul Cancro (AIRC) for a grant to G. Minchiotti, and the Centro Regionale di Competenza in Diagnostica e Farmaceutica Molecolari della Regione Campania for supporting a part of these activities are acknowledged. The technical support of Dr. Giuseppe Perretta is also gratefully acknowledged.

Supporting Information Available: Tables of chemical shifts for all four molecules. This material is available free of charge via the Internet at http://pubs.acs.org.

References

(1) Adkins, H. B.; Bianco, C.; Schiffer, S. G.; Rayhorn, P.; Zafari, M.; et al. Antibody blockade of the Cripto CFC domain suppresses tumor cell growth in vivo. *J. Clin. Invest.* **2003**, *112*, 575−587.
(2) Xing, P. X.; Hu, X. F.; Pietersz, G. A.; Hosick, H. L.; McKenzie, I. F. Cripto: a novel target for antibody-based cancer immunotherapy. *Cancer Res.* **2004**, *64*, 4018−4023.
(3) Bianco, C.; Strizzi, L.; Normanno, N.; Khan, N.; Salomon, D. S. Cripto-1: an oncofetal gene with many faces. *Curr. Top. Dev. Biol.* **2005**, *67*, 85−133.
(4) Hu, X. F.; Xing, P. X. Cripto as a target for cancer immunotherapy. *Expert Opin. Ther. Targets* **2005**, *9*, 383−394.
(5) Niemeyer, C. C.; Persico, M. G.; Adamson, E. D. Cripto: roles in mammary cell growth, survival, differentiation and transformation. *Cell Death Differ.* **1998**, *5*, 440−449.
(6) Xu, C.; Liguori, G.; Persico, M. G.; Adamson, E. D. Abrogation of the Cripto gene in mouse leads to failure of postgastrulation morphogenesis and lack of differentiation of cardiomyocytes. *Development* **1999**, *126*, 483−494.
(7) Salomon, D. S.; Bianco, C.; Ebert, A. D.; Khan, N. I.; De Santis, M.; et al. The EGF−CFC family: novel epidermal growth factor-related proteins in development and cancer. *Endocr.-Relat. Cancer* **2000**, *7*, 199−226.
(8) Sun, Y.; Strizzi, L.; Raafat, A.; Hirota, M.; Bianco, C.; et al. Overexpression of human Cripto-1 in transgenic mice delays mammary gland development and differentiation and induces mammary tumorigenesis. *Am. J. Pathol.* **2005**, *167*, 585−597.
(9) Wechselberger, C.; Strizzi, L.; Kenney, N.; Hirota, M.; Sun, Y.; et al. Human Cripto-1 overexpression in the mouse mammary gland results in the development of hyperplasia and adenocarcinoma. *Oncogene* **2005**, *24*, 4094−4105.
(10) Minchiotti, G.; Parisi, S.; Liguori, G. L.; D'Andrea, D.; Persico, M. G. Role of the EGF−CFC gene cripto in cell differentiation and embryo development. *Gene* **2002**, *287*, 33−37.
(11) Sonntag, K. C.; Simantov, R.; Bjorklund, L.; Cooper, O.; Pruszak, J.; et al. Context-dependent neuronal differentiation and germ layer induction of Smad4-/- and Cripto-/- embryonic stem cells. *Mol. Cell Neurosci.* **2005**, *28*, 417−429.
(12) Kenney, N. J.; Adkins, H. B.; Sanicola, M. Nodal and Cripto-1: embryonic pattern formation genes involved in mammary gland development and tumorigenesis. *J. Mammary Gland Biol. Neoplasia* **2004**, *9*, 133−144.
(13) Adamson, E. D.; Minchiotti, G.; Salomon, D. S. Cripto: a tumor growth factor and more. *J. Cell. Physiol.* **2002**, *190*, 267−278.
(14) Parisi, S.; D'Andrea, D.; Lago, C. T.; Adamson, E. D.; Persico, M. G.; et al. Nodal-dependent Cripto signaling promotes cardiomyogenesis and redirects the neural fate of embryonic stem cells. *J. Cell Biol.* **2003**, *163*, 303−314.
(15) Gerecht-Nir, S.; Dazard, J. E.; Golan-Mashiach, M.; Osenberg, S.; Botvinnik, A.; et al. Vascular gene expression and phenotypic correlation during differentiation of human embryonic stem cells. *Dev. Dyn.* **2005**, *232*, 487−497.
(16) Li, Y.; Powell, S.; Brunette, E.; Lebkowski, J.; Mandalam, R. Expansion of human embryonic stem cells in defined serum-free medium devoid of animal-derived products. *Biotechnol. Bioeng.* **2005**, *91*, 688−698.
(17) Liu, H.; Harris, T. M.; Kim, H. H.; Childs, G. Cardiac myocyte differentiation: the Nkx2.5 and Cripto target genes in P19 clone 6 cells. *Funct. Integr. Genomics* **2005**, *5*, 218−239.
(18) Minchiotti, G. Nodal-dependant Cripto signaling in ES cells: from stem cells to tumor biology. *Oncogene* **2005**, *24*, 5668−5675.
(19) Bianco, C.; Strizzi, L.; Ebert, A.; Chang, C.; Rehman, A.; et al. Role of human cripto-1 in tumor angiogenesis. *J. Natl. Cancer Inst.* **2005**, *97*, 132−141.
(20) Sakuma, R.; Ohnishi Yi, Y.; Meno, C.; Fujii, H.; Juan, H.; et al. Inhibition of Nodal signalling by Lefty mediated through interaction with common receptors and efficient diffusion. *Genes Cells* **2002**, *7*, 401−412.
(21) Yan, Y. T.; Liu, J. J.; Luo, Y.; E, C.; Haltiwanger, R. S.; et al. Dual roles of Cripto as a ligand and coreceptor in the nodal signaling pathway. *Mol. Cell Biol.* **2002**, *22*, 4439−4449.
(22) Yeo, C.; Whitman, M. Nodal signals to Smads through Cripto-dependent and Cripto-independent mechanisms. *Mol. Cell* **2001**, *7*, 949−957.
(23) Schier, A. F. Nodal signaling in vertebrate development. *Annu. Rev. Cell Dev. Biol.* **2003**, *19*, 589−621.
(24) Chen, C.; Ware, S. M.; Sato, A.; Houston-Hawkins, D. E.; Habas, R.; et al. The Vg1-related protein Gdf3 acts in a Nodal signaling pathway in the pre-gastrulation mouse embryo. *Development* **2006**, *133*, 319−329.
(25) Cheng, S. K.; Olale, F.; Bennett, J. T.; Brivanlou, A. H.; Schier, A. F. EGF−CFC proteins are essential coreceptors for the TGF-beta signals Vg1 and GDF1. *Genes Dev.* **2003**, *17*, 31−36.
(26) Gray, P. C.; Harrison, C. A.; Vale, W. Cripto forms a complex with activin and type II activin receptors and can block activin signaling. *Proc. Natl. Acad. Sci. U.S.A.* **2003**, *100*, 5193−5198.
(27) Cheng, S. K.; Olale, F.; Brivanlou, A. H.; Schier, A. F. Lefty blocks a subset of TGFbeta signals by antagonizing EGF−CFC coreceptors. *PLoS Biol.* **2004**, *2*, E30.
(28) Bianco, C.; Strizzi, L.; Rehman, A.; Normanno, N.; Wechselberger, C.; et al. A Nodal- and ALK4-independent signaling pathway activated by Cripto-1 through Glypican-1 and c-Src. *Cancer Res.* **2003**, *63*, 1192−1197.
(29) Lohmeyer, M.; Harrison, P. M.; Kannan, S.; DeSantis, M.; O'Reilly, N. J.; et al. Chemical synthesis, structural modeling, and biological activity of the epidermal growth factor-like domain of human cripto. *Biochemistry* **1997**, *36*, 3837−3845.
(30) Foley, S. F.; van Vlijmen, H. W.; Boynton, R. E.; Adkins, H. B.; Cheung, A. E.; et al. The CRIPTO/FRL-1/CRYPTIC (CFC) domain of human Cripto. Functional and structural insights through disulfide structure analysis. *Eur. J. Biochem.* **2003**, *270*, 3610−3618.
(31) Marasco, D.; Saporito, A.; Ponticelli, S.; Chambery, A.; De Falco, S.; et al. Chemical synthesis of mouse cripto CFC variants. *Proteins* **2006**, *64*, 779−788.
(32) Risbridger, G. P.; Schmitt, J. F.; Robertson, D. M. Activins and inhibins in endocrine and other tumors. *Endocr. Rev.* **2001**, *22*, 836−858.
(33) Shen, M. M. Decrypting the role of Cripto in tumorigenesis. *J. Clin. Invest.* **2003**, *112*, 500−502.
(34) Bianco, C.; Normanno, N.; Salomon, D. S.; Ciardiello, F. Role of the cripto (EGF-CFC) family in embryogenesis and cancer. *Growth Factors* **2004**, *22*, 133−139.
(35) Hu, X. F.; Xing, P. X. Cripto monoclonal antibodies. *Drug News Perspect.* **2005**, *18*, 293−303.
(36) Shen, M. M.; Schier, A. F. The EGF−CFC gene family in vertebrate development. *Trends Genet.* **2000**, *16*, 303−309.
(37) Persico, M. G.; Liguori, G. L.; Parisi, S.; D'Andrea, D.; Salomon, D. S.; et al. Cripto in tumors and embryo development. *Biochim. Biophys. Acta* **2001**, *1552*, 87−93.
(38) Wishart, D. S.; Sykes, B. D.; Richards, F. M. Relationship between nuclear magnetic resonance chemical shift and protein secondary structure. *J. Mol. Biol.* **1991**, *222*, 311−333.
(39) Guntert, P.; Mumenthaler, C.; Wuthrich, K. Torsion angle dynamics for NMR structure calculation with the new program DYANA. *J. Mol. Biol.* **1997**, *273*, 283−298.
(40) Harrison, P. M.; Sternberg, M. J. E. The disulphide beta-cross: from cystine geometry and clustering to classification of small disulphide-rich protein folds. *J. Mol. Biol.* **1996**, *264*, 603−623.

(41) Minchiotti, G.; Parisi, S.; Liguori, G.; Signore, M.; Lania, G. et al. Membrane-anchorage of Cripto protein by glycosylphosphatidylinositol and its distribution during early mouse development. *Mech. Dev.* **2000**, *90*, 133−142.
(42) Shi, S.; Stanley, P. Protein *O*-fucosyltransferase 1 is an essential component of Notch signaling pathways. *Proc. Natl. Acad. Sci. U.S.A.* **2003**, *100*, 5234−5239.
(43) Schiffer, S. G.; Foley, S.; Kaffashan, A.; Hronowski, X.; Zichittella, A. E.; et al. Fucosylation of Cripto is required for its ability to facilitate nodal signaling. *J. Biol. Chem.* **2001**, *276*, 37769−37778.
(44) Bax, A.; Davis, D. G. MLEV-17-based two-dimensional homonuclear magnetization transfer spectroscopy. *J. Magn. Res.* **1985**, *65*, 355−360.
(45) Bax, A. Practical aspects of two-dimensional transverse NOE spectroscopy. *J. Magn. Res.* **1985**, *63*, 207−213.
(46) Piantini, U.; Sorensen, O. W.; Ernst, R. R. Multiple quantum filters for elucidating NMR coupling networks. *J. Am. Chem. Soc.* **1982**, *104*, 6800−6801.
(47) States, D. J.; Haberhorn, R. A.; Ruben, D. J. A two-dimensional nuclear Overhauser experiment with pure absorption phase in four quadrants. *J. Magn. Res.* **1982**, *48*, 286−292.
(48) Piotto, M.; Saudek, V.; Skelnar, V. J. Gradient-tailored excitation for single-quantum NMR spectroscopy of aqueous solutions. *J. Biomol. NMR* **1992**, *2*, 661−665.
(49) Delaglio, F.; Grzesiek, S.; Vuister, G. W.; Zhu, G.; Pfeifer, J.; et al. NMRPipe: a multidimensional spectral processing system based on UNIX pipes. *J. Biomol. NMR* **1995**, *6*, 277−293.
(50) Johnson, B. A.; Blevins, R. A. NMRView: A computer program for the visualization and analysis of NMR data. *J. Biomol. NMR* **1994**, *4*, 603−614.
(51) Wuthrich, K. *NMR of Proteins and Nucleic Acids*; Wiley: New York, 1986.
(52) Guntert, P.; Braun, W.; Wuthrich, K. Efficient computation of three-dimensional protein structures in solution from nuclear magnetic resonance data using the program DIANA and the supporting programs CALIBA, HABAS, and GLOMSA. *J. Mol. Biol.* **1991**, *217*, 517−530.
(53) Karplus, M. Vicinal proton coupling in nuclear magnetic resonance. *J. Am. Chem. Soc.* **1963**, *85*, 2870−2871.
(54) Guntert, P.; Wuthrich, K. Improved efficiency of protein structure calculations from NMR data using the program DIANA with redundant dihedral angle constraints. *J. Biomol. NMR* **1991**, *1*, 447−456.
(55) Case, D. A.; Pearlman, D. A.; Caldwell, J. W.; Cheatham, I. T. E.; Ross, W. S.; et al. *AMBER 6*; University of California: San Francisco, CA, 1999.
(56) Pearlman, D. A.; Case, D. A.; Caldwell, J. W.; Ross, W. S.; Cheatham, I. T. E.; et al. AMBER, a package of computer programs for applying molecular mechanics, normal mode analysis, molecular dynamics and free energy calculations to stimulate the structural and energetic properties of molecules. *Proteins* **1996**, *26*, 304−313.
(57) Weiner, S. J.; Kollmann, P. A.; Nguyen, D. T.; Case, D. A. An all atom force field for simulations of proteins and nucleic acids. *J. Comput. Chem.* **1986**, *7*, 230−238.
(58) Koradi, R.; Billeter, M.; Wuthrich, K. MOLMOL: a program for display and analysis of macromolecular structures. *J. Mol. Graphics Modell.* **1996**, *14*, 51−55.

JM060772R